

# Geophysical Research Letters

## RESEARCH LETTER

10.1029/2018GL080554

### Key Points:

- Subpolar North Atlantic winter surface ocean  $f\text{CO}_2$  growth rates track the atmospheric  $\text{CO}_2$  growth rate between 2004 and 2017
- DIC-driven  $f\text{CO}_2$  changes are twice as large as expected from atmospheric trends in  $f\text{CO}_2$ , a result of substantial surface cooling
- Interannual  $f\text{CO}_2$  variability in the Irminger Sea is linked to mixed layer depth and the North Atlantic Oscillation

### Supporting Information:

- Supporting Information S1

### Correspondence to:

F. Fröb and A. Olsen,  
friederike.froeb@mpimet.mpg.de;  
are.olsen@uib.no

### Citation:

Fröb, F., Olsen, A., Becker, M., Chafik, L., Johannessen, T., Reverdin, G., & Omar, A. (2019). Wintertime  $f\text{CO}_2$  variability in the subpolar North Atlantic since 2004. *Geophysical Research Letters*, 46, 1580–1590. <https://doi.org/10.1029/2018GL080554>


Received 19 SEP 2018

Accepted 29 JAN 2019

Accepted article online 31 JAN 2019

Published online 14 FEB 2019

## Wintertime $f\text{CO}_2$ Variability in the Subpolar North Atlantic Since 2004

F. Fröb<sup>1,2</sup> , A. Olsen<sup>1</sup> , M. Becker<sup>1</sup> , L. Chafik<sup>1,3</sup> , T. Johannessen<sup>1,4</sup>, G. Reverdin<sup>5</sup> , and A. Omar<sup>4</sup>

<sup>1</sup>Geophysical Institute and Bjerknes Centre for Climate Research, University of Bergen, Bergen, Norway, <sup>2</sup>Now at Max Planck Institute for Meteorology, Hamburg, Germany, <sup>3</sup>Department of Meteorology and Bolin Centre for Climate Research, Stockholm University, Stockholm, Sweden, <sup>4</sup>NORCE Norwegian Research Centre AS and Bjerknes Centre for Climate Research, Bergen, Norway, <sup>5</sup>Sorbonne-Université, CNRS/IRD/MNHN (LOCEAN), Paris, France

**Abstract** Winter data of surface ocean temperature (SST), salinity (SSS) and  $\text{CO}_2$  fugacity ( $f\text{CO}_2$ ) collected on the VOS M/V Nuka Arctica in the subpolar North Atlantic between 2004 and 2017 are used to establish trends, drivers, and interannual variability. Over the period, waters cooled and freshened, and the  $f\text{CO}_2$  increased at a rate similar to the atmospheric  $\text{CO}_2$  growth rate. When accounting for the freshening, the inferred increase in dissolved inorganic carbon (DIC) was found to be approximately twice that expected from atmospheric  $\text{CO}_2$  alone. This is attributed to the cooling. In the Irminger Sea,  $f\text{CO}_2$  exhibited additional interannual variations driven by atmospheric forcing through winter mixing. As winter  $f\text{CO}_2$  in the region is close to the atmospheric, the subpolar North Atlantic has varied between being slightly supersaturated and slightly undersaturated over the investigated period.

**Plain Language Summary** The global oceans take up roughly a quarter of carbon dioxide ( $\text{CO}_2$ ) from fossil fuels and industry per year. As the emissions of  $\text{CO}_2$  increase, the amount of  $\text{CO}_2$  taken up by the oceans should increase in proportion; however, the ability of the ocean to remove  $\text{CO}_2$  from the atmosphere varies on interannual to decadal time scales. Here we assess processes that drive short-term variability and long-term trends of the subpolar North Atlantic carbon sink based on observational data obtained during winters between 2004 and 2017. We find that the subpolar North Atlantic has indeed kept pace with rising emissions over the entire period of time, which was mainly attributed to solubility-driven uptake of  $\text{CO}_2$ . Year-to-year changes of the surface ocean partial pressure of  $\text{CO}_2$  can be linked to the depth of the winter mixed layer as well as atmospheric forcing. In general, the North Atlantic has shifted between a small source and a small sink of atmospheric  $\text{CO}_2$  during wintertime. Our results underline the need to maintain long-term physical, chemical, and biological observations in order to monitor the ocean  $\text{CO}_2$  sink and understand the processes driving variability.

## 1. Introduction

All signatory parties of the 2015 Paris Agreement vetted at COP21 (United Nations Framework Convention on Climate Change, 2015) pledged to curb their carbon dioxide ( $\text{CO}_2$ ) emissions so that the global mean temperature increase until the end of this century will not exceed 2 °C above preindustrial levels. Continued and internationally coordinated observations of the global carbon cycle are needed to ensure that the reduction efforts are indeed effective (Marotzke et al., 2017). Data currently collected allow, for example, the preparation of the annual global carbon budget across atmosphere, ocean, and land sinks (Le Quéré et al., 2018). As the global oceans constitute the largest sustained sink for anthropogenic  $\text{CO}_2$  (Wanninkhof et al., 2013), long-term observations of seawater  $\text{CO}_2$  chemistry are essential to quantify the magnitude and variability on interannual to longer time scales of the oceanic  $\text{CO}_2$  uptake efficiency (Heinze et al., 2015).

Regular observations have been obtained in many ocean regions for multiple decades, in particular since the early 2000s with the increased accessibility of underway  $p\text{CO}_2$  instrumentation (Bakker et al., 2016; Pierrot et al., 2009). These observations show that globally, the long-term trends in surface ocean  $\text{CO}_2$  are similar to but slightly less than the atmospheric  $\text{CO}_2$  trends (Fay & McKinley, 2013; Landschützer et al., 2016; McKinley et al., 2011; Takahashi et al., 2009). However, they also reveal significant interannual and decadal variability in the ocean sink strength, globally (Landschützer et al., 2016; Rödenbeck et al., 2014,

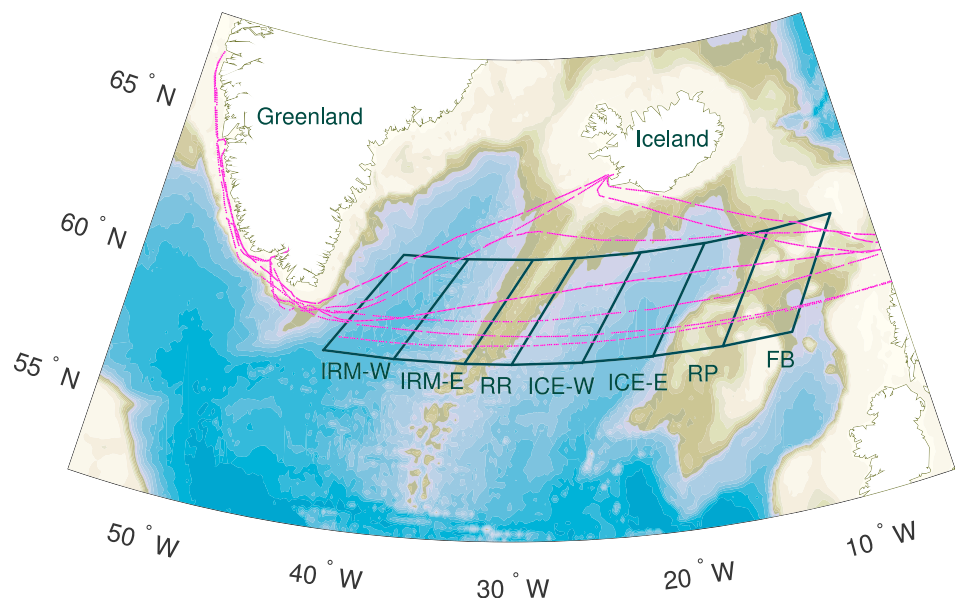


**Figure 1.** Map of the subpolar North Atlantic. For clarity, only example tracks of M/V Nuka Arctica are shown (pink lines). The track is divided into seven boxes: Irminger Sea West and East (IRM-W and IRM-E), Reykjanes Ridge (RR), Iceland Basin West and East (ICE-W and ICE-E), the Rockall Plateau (RP), and the Faroer Bank (FB). The filled contours show the bathymetry at 250-m steps.

2015) and regionally (e.g., Corbière et al., 2007; Landschützer et al., 2015; Metzl et al., 2010; Schuster & Watson, 2007). Ocean circulation change in response to atmospheric forcing is an important driver of such surface ocean  $\text{CO}_2$  variability, for example, in the equatorial Pacific (e.g., Feely et al., 2006; Rödenbeck et al., 2014), the Southern Ocean (Landschützer et al., 2015; Le Quéré et al., 2007; Lovenduski et al., 2007), and the North Atlantic (e.g., Gruber, 2009).

The North Atlantic is among the world's largest sinks for atmospheric  $\text{CO}_2$  (Takahashi et al., 2009) with substantial interannual to decadal variability (e.g., Gruber et al., 2002; Landschützer et al., 2013; McKinley et al., 2011). Observations suggest a considerable increase in  $f\text{CO}_2$  from the 1990s to the late 2000s in the subpolar gyre, such that surface ocean  $\text{CO}_2$  trends diverged from the atmospheric trends (Corbière et al., 2007; Metzl et al., 2010). The increase in surface  $f\text{CO}_2$  between 1993 and 2003 has been attributed to a strong surface warming associated with a weaker state of the North Atlantic Oscillation (NAO) and a contracted subpolar gyre (Corbière et al., 2007; McKinley et al., 2011), which led to little or no increase in dissolved inorganic carbon (DIC; Corbière et al., 2007; Thomas et al., 2008). In the later period, that is, 2001 to 2008, the measured surface  $f\text{CO}_2$  trends accelerated, which according to Metzl et al. (2010) were not primarily driven by anthropogenic  $\text{CO}_2$  uptake. Instead, the accumulation of DIC was accompanied by an increase in nutrients in Redfield proportions, which is suggestive of a mechanism involving variations in vertical mixing processes and ventilation patterns. However, a firm connection between vertical mixing and surface  $\text{CO}_2$  variations has not yet been established from observations in this region.

In this study, the spatiotemporal variability of subpolar North Atlantic surface ocean  $f\text{CO}_2$  is analyzed beyond the period explored by Corbière et al. (2007) and Metzl et al. (2010). A total of 14 years of data, collected in the North Atlantic on board the voluntary observing ship (VOS) Nuka Arctica (Olsen et al., 2008), allow to resolve regional aspects of wintertime  $f\text{CO}_2$  trends between 2004 and 2017 along with their underlying drivers. Interannual variations of surface ocean  $f\text{CO}_2$  are also evaluated, with the aim to identify the relation between  $f\text{CO}_2$  and vertical mixing, especially since recurring deep convection has been observed in winters since 2008 (de Jong & de Steur, 2016; Fröb et al., 2016; Piron et al., 2017; Våge et al., 2009).

## 2. Data

The container vessel M/V Nuka Arctica, owned by Royal Arctic Line, operates between Ilulissaat, Greenland and Aalborg, Denmark. The ship crosses the North Atlantic directly at approximately  $59^\circ\text{N}$ , but changes the track depending on the sailing schedule and the weather. Example ship tracks are shown in Figure 1,

while all tracks relevant for this study are presented in the supporting information Figure S1. Throughout the years the system setup has remained similar to the one described by Olsen et al. (2008), apart from a relocation from the bow-thruster cavity to the main-engine room in early 2006, in order to minimize the number of air bubbles in the seawater stream. There has been no shift in observed  $f\text{CO}_2$  attributed to the relocation of the instrument as shown in the supporting information (Figure S2). The intake is located approximately 5 m beneath the water line with a main seawater inflow of  $\approx 60$  L/min, of which  $\sim 2$  L/min are teed off to the  $f\text{CO}_2$  instrument, while the remainder is directed to the thermosalinograph and then overboard. The sea surface temperature (SST) is measured with an accuracy of  $0.01$  °C using a regularly calibrated thermometer, which is installed right downstream of the intake valve. All pipes are insulated with styrofoam and the typical warming between the intake and equilibrator temperature is not larger than  $0.5$  °C, which is corrected for using the empirical relationship of Takahashi et al. (1993) of  $0.0423$  °C<sup>-1</sup>. The uncertainty of  $f\text{CO}_2$  measurements on Nuka Arctica is  $\pm 2$   $\mu\text{atm}$ . Data are available through the Surface Ocean CO<sub>2</sub> Atlas (SOCAT) database (Bakker et al., 2016) and the Integrated Carbon Observation System (ICOS)-Norway website (<https://no.icos-cp.eu>). Here, only winter data, that is, December to March, from January 2004 to March 2017 are analyzed in order to minimize the potential impact of biological activity, which has been shown to be highly variable in timing and magnitude on interannual time scales in the subpolar North Atlantic (Henson et al., 2006, 2013).

Sea surface salinity (SSS) is measured by a SBE-21 Seacat thermosalinograph. Data indicative of too weak flow speeds or bubbles in the water flow have been excluded (approximately 20%). The remaining data were calibrated following Alory et al. (2015), using in situ water samples collected across the Atlantic and analyzed for salinity at the Greenland Institute of Natural Resources, Nuuk, Greenland, and also using salinity values flagged as “good” from nearby Argo floats. The typical range of these salinity corrections are 0 to  $-0.6$  (Reverdin et al., 2018).

Monthly mean atmospheric CO<sub>2</sub> mole fraction data were provided by the Cooperative Global Atmospheric Data Integration Project (2016). Here, the monthly  $x\text{CO}_2$  data collected at Storholti, Iceland ( $63.3^\circ\text{N}$ ) and Mace Head, Ireland ( $53.3^\circ\text{N}$ ) were used and linearly interpolated in order to resolve latitudinal gradients. The  $x\text{CO}_2$  data were converted to fugacity at 100% humidity following Weiss and Price (1980).

The strong correlation between sea surface alkalinity ( $A_t$ ) and SSS in the open ocean can be described by an empirical relationship of the form  $A_t = m_{\text{SSS}} \times \text{SSS} + n$  (Friis et al., 2003; Millero et al., 1998). Here, the following precision-adjusted relationship for the North Atlantic was used to approximate  $A_t$  (Nondal et al., 2009, only one significant digit is included here):

$$A_t = 49.4\mu\text{mol/kg} \times \text{SSS} + 582.0\mu\text{mol/kg}; (\text{SSS} > 34.5) \quad (1)$$

The seawater CO<sub>2</sub> chemistry can be described with the measured  $f\text{CO}_2$  data and  $A_t$  derived from salinity, using the dissociation constants of Lueker et al. (2000) as implemented in CO<sub>2</sub>SYS (Lewis & Wallace, 1998; van Heuven et al., 2011). The  $A_t$ -SSS relationship and the approximation of DIC, derived from calculated  $A_t$  and measured  $f\text{CO}_2$ , were validated using 310 surface  $A_t$ , DIC, and  $f\text{CO}_2$  measurements, collected in the Iceland Basin and the Irminger Sea in April 2015, on board R/V G.O. Sars (58GS20150410). The mean difference between measured and calculated  $A_t$  was  $0.3 \pm 4.2$   $\mu\text{mol/kg}$ , while the mean difference between measured and calculated DIC was  $0.9 \pm 9.1$   $\mu\text{mol/kg}$ . The residuals for both calculated  $A_t$  and calculated DIC are shown in the supporting information (Figures S3 and S4), and no bias is evident.

### 3. Methods

#### 3.1. Computation of Regional Trends

Trends in measured  $f\text{CO}_2$  were determined for seven different boxes along the tracks of Nuka Arctica. The north-south boundaries of each box were set to  $61.5^\circ\text{N}$  and  $58^\circ\text{N}$  in order to minimize the effects of latitudinal gradients of  $f\text{CO}_2$ , while the east-west boundaries were oriented parallel to the Reykjanes Ridge, as shown in Figure 1, to align with the direction of ocean currents (Chafik et al., 2014; Knutsen et al., 2005). The box over the Reykjanes Ridge (RR) is  $3^\circ$  wide in longitude and its eastern and western boundaries follow the  $\sim 1,500$  m isobath. To the west, the Irminger Sea was divided into two boxes (IRM-W and IRM-E), each  $4.5^\circ$  wide in longitude. The western boundary of IRM-W follows approximately the  $\sim 2,500$  m isobath, while the division between IRM-W and IRM-E was set approximately at the eastern  $\sim 3,000$  m isobath. East of the Reykjanes Ridge, all four boxes are  $4.5^\circ$  wide in longitude. The Iceland Basin was divided into a western box (ICE-W), which covers the slope from  $\sim 1,500$ - to  $\sim 2,500$  m depth from west to east, and an eastern

box (ICE-E), whose boundaries follow the  $\sim 2,500$  m isobath. The box to the east of ICE-E covers the ascent to the Hatton Bank and the Rockall Plateau (RP), which is about  $\sim 1,000$  m deep, and the easternmost box covers the shallow area close the Faroe Bank (FB).

Regional trends were computed by deseasonalizing all data following Tjiputra et al. (2014). For every region and year, the respective monthly mean values were computed for 2004 to 2017. From these monthly means, the 14-year monthly means were subtracted. Regional winter trends were calculated by applying a linear regression over the deseasonalized December to March data. The standard error of the slope is the error of the trend estimate. Deseasonalization is necessary, because  $f\text{CO}_2$  was not measured with the same frequency for every month, year, and region. Table S1 in the supporting information shows the number of observations per region and winter.

### 3.2. Decomposition of Surface $f\text{CO}_2$ Trends

The trend in sea surface  $f\text{CO}_2$  is driven by changes in SST, SSS,  $A_t$ , and DIC. The main drivers for the observed changes can be identified by decomposing the  $f\text{CO}_2$  trend, while explicitly accounting for freshwater impacts on DIC and  $A_t$  (Keeling et al., 2004; Lovenduski et al., 2007; Takahashi et al., 1993):

$$\begin{aligned} \frac{df\text{CO}_2}{dt} = & \tau \langle f\text{CO}_2 \rangle \frac{d\text{SST}}{dt} + \eta \frac{\langle f\text{CO}_2 \rangle}{\langle \text{SSS} \rangle} \frac{d\text{SSS}}{dt} + \gamma \frac{\langle f\text{CO}_2 \rangle}{\langle \text{DIC} \rangle} \left( \frac{\langle s\text{DIC} \rangle}{\text{SSS}_0} \frac{d\text{SSS}}{dt} + \frac{\langle \text{SSS} \rangle}{\text{SSS}_0} \frac{ds\text{DIC}}{dt} \right) \\ & + \Gamma \frac{\langle f\text{CO}_2 \rangle}{\langle A_t \rangle} \left( \frac{\langle sA_t \rangle}{\text{SSS}_0} \frac{d\text{SSS}}{dt} + \frac{\langle \text{SSS} \rangle}{\text{SSS}_0} \frac{dsA_t}{dt} \right) \end{aligned} \quad (2)$$

Here,  $\langle X \rangle$  are mean winter, that is, December to March, values of  $f\text{CO}_2$ , SST, SSS, DIC, or  $A_t$ .  $\text{SSS}_0$  is the reference salinity, which is set to 35 (Normal Standard Seawater, Millero et al., 2008).  $s\text{DIC}$  and  $sA_t$  were computed by normalizing DIC and  $A_t$  to a salinity of 35 and assuming a nonzero freshwater endmember DIC and  $A_t$  concentration equal to the intercept of equation (1) (Friis et al., 2003). The trends of  $dX/dt$  were estimated from 2004 to 2017 for each of the seven regions. The parameter  $\tau$  is  $0.0423 \text{ }^\circ\text{C}^{-1}$  (Takahashi et al., 1993). Averaged over all boxes,  $\eta$  is 0.91, which was estimated as  $\partial f\text{CO}_2 / \partial \text{SSS} \times \langle \text{SSS} \rangle / \langle f\text{CO}_2 \rangle$ .  $\gamma$  is the Revelle factor for DIC (on average 13.16) as calculated using CO2SYS (Lewis & Wallace, 1998; van Heuven et al., 2011). Finally,  $\Gamma$  is the Revelle factor for  $A_t$  (on average -11.76), which was estimated at constant DIC as  $\partial f\text{CO}_2 / \partial A_t \times \langle A_t \rangle / \langle f\text{CO}_2 \rangle$  and as such additionally implemented in CO2SYS for this purpose.  $\eta$ ,  $\gamma$ , and  $\Gamma$  were calculated for each region based on long-term mean winter values.

## 4. Long-Term Trends and Drivers

The regional trends of measured  $f\text{CO}_2$  in the ocean ( $f\text{CO}_2^{\text{oc}}$ ) and the atmosphere ( $f\text{CO}_2^{\text{atm}}$ ) are presented in Figure 2a as well as in the supplementary material (Figure S5). The ocean is keeping pace with rising  $\text{CO}_2$  emissions if the trend in  $f\text{CO}_2^{\text{oc}}$  equals the  $f\text{CO}_2^{\text{atm}}$  trend. As long as the growth rate in  $f\text{CO}_2^{\text{oc}}$  is larger or smaller than in  $f\text{CO}_2^{\text{atm}}$ , the uptake of atmospheric  $\text{CO}_2$  is not constant over time. Taking the standard error of the growth rates in to account,  $f\text{CO}_2^{\text{oc}}$  tracks the atmospheric growth rate of  $2.0 \pm 0.0 \text{ } \mu\text{atm}/\text{year}$  in all boxes except the FB. The  $f\text{CO}_2^{\text{oc}}$  trend gradually increases toward the east from  $1.96 \pm 0.27 \text{ } \mu\text{atm}/\text{year}$  in the IRM-W box to  $2.27 \pm 0.14 \text{ } \mu\text{atm}/\text{year}$  in the FB box. The trends in surface  $s\text{DIC}$  are not significantly different from each other (Figure 2b) and averaged over all boxes,  $s\text{DIC}$  has increased by  $1.56 \pm 0.20 \text{ } \mu\text{mol}\cdot\text{kg}^{-1}\cdot\text{year}^{-1}$ .

The SST measurements on Nuka Arctica show a substantial cooling during winters between 2004 and 2017 (Figures 2c and S6). From the IRM-W to the ICE-W box, the SST trend varies between  $-0.084 \pm 0.020$  and  $-0.096 \pm 0.018 \text{ }^\circ\text{C}/\text{year}$ . Toward the east, the cooling is less pronounced, and in the FB box, the SST trend is only  $-0.045 \pm 0.016 \text{ }^\circ\text{C}/\text{year}$ . Averaged over all boxes, SST decreased by  $0.78 \pm 0.19 \text{ }^\circ\text{C}$  per decade.

Coinciding with the basin-wide cooling, the subpolar North Atlantic has freshened from 2004 to 2017 (Figures 2d and S7). The decline in SSS measured on Nuka Arctica is strongest in the Iceland Basin. Here, SSS declined by  $25.6 \pm 4.1 \times 10^{-3} \text{ year}^{-1}$  (ICE-W) and  $19.8 \pm 4.0 \times 10^{-3} \text{ year}^{-1}$  (ICE-E). Toward the west and east, the freshening trends are less pronounced. In the IRM-W, the freshening trend is not significant ( $1.0 \pm 2.0 \times 10^{-3} \text{ year}^{-1}$ ), but the IRM-E box freshens slightly, at a rate of  $10.6 \pm 2.5 \times 10^{-3} \text{ year}^{-1}$ . In the FB region, the SSS change is significantly different from zero but relatively modest ( $-6.8 \pm 3.3 \times 10^{-3} \text{ year}^{-1}$ ). Averaged over all boxes, SSS decreased by  $13.4 \pm 3.1 \times 10^{-3} \text{ year}^{-1}$ .

In Figure 2e, the individual contributions of SST, SSS, DIC, and  $A_t$  changes to the  $f\text{CO}_2$  trends are presented for all boxes, as well as the actual observed trend in  $f\text{CO}_2$ . The effects of DIC on  $f\text{CO}_2^{\text{oc}}$  are separated into

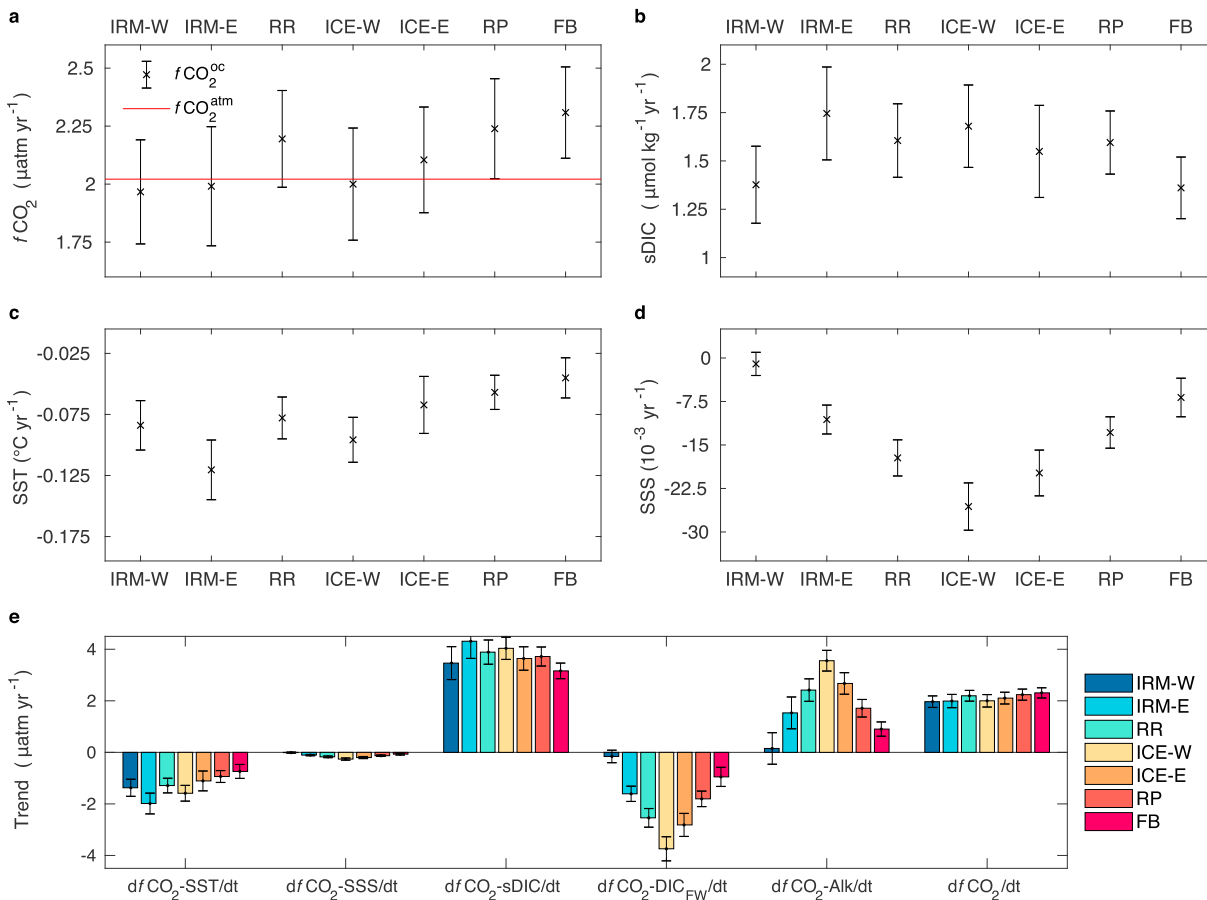


**Figure 2.** Regional trend estimates based on deseasonalized winter data from 2004 to 2017 for (a)  $f\text{CO}_2^{\text{oc}}$  (black crosses) and  $f\text{CO}_2^{\text{atm}}$  (red solid line), (b)  $\text{sDIC}$ , (c) SST, and (d) SSS. The error bars represent the error of the linear regression model. (e) Decomposition of surface  $f\text{CO}_2$  trends according to equation (2). The effect of regional changes in SST, SSS,  $\text{sDIC}$ ,  $\text{DIC}_{\text{FW}}$  and  $A_t$  on the regional  $f\text{CO}_2$  trends is shown. The  $\text{d}f\text{CO}_2/\text{d}t$  is the observed trend in  $f\text{CO}_2$ . DIC = dissolved inorganic carbon (DIC); IRM-W and IRM-E = Irminger Sea West and East; RR = Reykjanes Ridge; ICE-W and ICE-E = Iceland Basin West and East; RP = Rockall Plateau; FB = Faroer Bank.

those driven by biogeochemical processes (i.e., air-sea gas exchange, primary production, entrainment of waters rich in DIC from below),  $\text{d}f\text{CO}_2\text{-sDIC}/\text{d}t$ , and those associated with salinity changes (i.e., freshwater addition/removal leading to dilution/concentration of DIC),  $\text{d}f\text{CO}_2\text{-DIC}_{\text{FW}}/\text{d}t$ . For alkalinity, no such separation can be made. As a direct consequence of the empirical relationship between  $A_t$  and SSS by Nondal et al. (2009) and the approach by Friis et al. (2003) to calculate  $sA_t$ , the trend in  $sA_t$  is zero, and therefore, so is the biogeochemical  $A_t$  driver.

The observed trends in  $f\text{CO}_2$  are generally well reproduced by the decomposition. The sum of the drivers for all regions are compared to the observed  $f\text{CO}_2$  trends in the supporting information Figure S8. Differences between the observed trend and the summed effects of SST, SSS, DIC, and  $A_t$  changes may reflect contributions of nonlinearities in the seawater  $\text{CO}_2$  chemistry. In all boxes, these differences are not statistically significant and smaller than 10% except in the RP box, where the sum of all drivers is  $14 \pm 30\%$  larger than the observed trend in  $f\text{CO}_2$ . For all boxes, the contributions of freshwater-driven changes in DIC and  $A_t$  changes balance out; that is, DIC and  $A_t$  are diluted in equal parts. As the freshening is strongest in the Iceland Basin,  $\text{DIC}_{\text{FW}}$  and  $A_{t,\text{FW}}$  are largest in ICE-W and ICE-E. It is in these two boxes where the contributions of SSS changes to the trend in  $f\text{CO}_2$  are strongest, yet they are insignificant compared to all other contributions. The  $\text{sDIC}$ -driven  $f\text{CO}_2$  growth rate is twice as high, in some regions even higher, than expected for an ocean that tracks the atmospheric  $\text{CO}_2$  increase,  $2.0 \mu\text{atm}/\text{year}$ . This is attributed to the cooling-induced increase in  $\text{CO}_2$  solubility. The regional gradient in  $\text{sDIC}$ -driven changes in  $f\text{CO}_2$  is opposite to that of SST-driven  $f\text{CO}_2$  changes, which additionally confirms the solubility-driven uptake of  $\text{CO}_2$ .

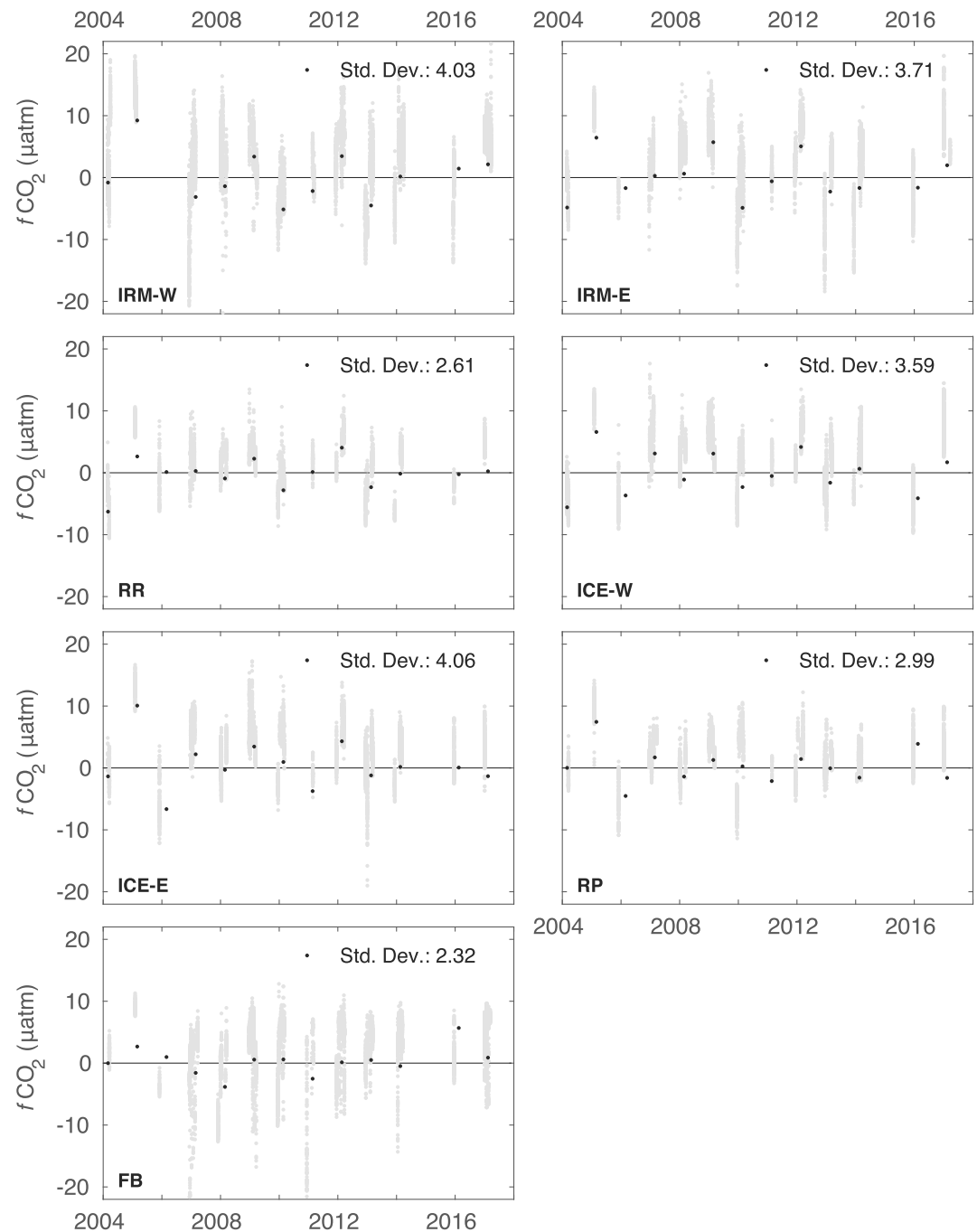


**Figure 3.** Winter mean of detrended  $f\text{CO}_2$  data between 2004 and 2017 for all regions (black dots). To obtain the detrended time series, the trend over all deseasonalized  $f\text{CO}_2$  data was removed. Gray dots in the background show all detrended December to March data. Interannual variability is indicated by the standard deviation of the winter mean values. IRM-W and IRM-E = Irminger Sea West and East; RR = Reykjanes Ridge; ICE-W and ICE-E = Iceland Basin West and East; RP = Rockall Plateau; FB = Faroer Bank.

### 5. Interannual Variation of $f\text{CO}_2$

On average, wintertime  $f\text{CO}_2$  across the track of Nuka is the same as the atmosphere (Figure S5). The year-to-year variation of the measured  $f\text{CO}_2$  data is evaluated by removing the observed trend in each region between 2004 and 2017 from the deseasonalized  $f\text{CO}_2$  data (Figure 3). As a measure of interannual variability, the standard deviation of the mean detrended winter values is used. As a consequence of the  $f\text{CO}_2$  trend in the surface ocean tracking the atmospheric  $\text{CO}_2$  growth rate between 2004 and 2017, conditions in the

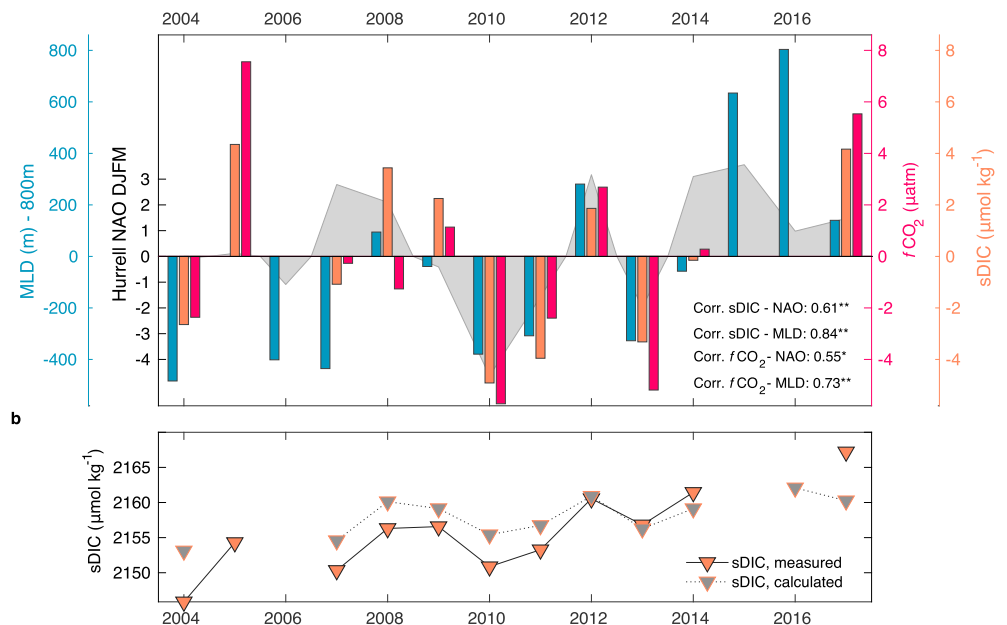


**Figure 4.** (a) Left axis: Background filled contour shows in gray the December to March (DJFM) North Atlantic Oscillation (NAO) index (Hurrell & National Center for Atmospheric Research Staff (Eds), 2017). The blue bars show maximum winter mixed layer depth (MLD) anomaly with respect to 800 m. Right axis: Detrended data of January to March sDIC (orange bars) and  $f\text{CO}_2$  (red bars) in the IRM-W region. The indicated correlations are significant with  $p$  values smaller than 0.05 (\*\*) and smaller than 0.10 (\*). Note that in the IRM-W region no Argo float data were available in 2005 and no sDIC and  $f\text{CO}_2$  data were available in 2006, 2015, and 2016. (b) Detrended data of sDIC (orange triangles) based on Nuka data and calculated sDIC (gray triangles) based on the one-dimensional box model (see supporting information for further details). The root-mean-square error is  $5.8 \mu\text{mol/kg}$ . DIC = dissolved inorganic carbon; IRM-W = Irminger Sea West.

subpolar North Atlantic during winter shift to a varying extent between supersaturation and undersaturation with respect to atmospheric  $\text{CO}_2$ . Consistent over all regions, detrended  $f\text{CO}_2$  values of data collected in 2005 are much larger than those in 2004, but dropped again in winter 2006. As the  $f\text{CO}_2$  system was installed in the bow-thruster cavity in both 2004 and 2005, this drop into 2006 is most likely not related to the relocation of the installation to the main-engine room, but a real signal of interannual variability. Instances of particularly low detrended  $f\text{CO}_2$  values can be linked to the intrusion of water masses with a different salinity and temperature signature. For example, the low values in the IRM-W box in 2007 can be attributed to abnormal presence of relatively cold and fresh Greenland shelf waters (Henson et al., 2013) and similarly, the low  $f\text{CO}_2$  levels in the FB box in 2007 and 2011 are associated with cool waters from the Faroe Shelf spilling into the study area.

While the large interannual variability of the detrended  $f\text{CO}_2$  measurements in the Iceland Basin is likely related to high interannual in SSS (Figure S7), in the Irminger Sea, it is indicative of the influence of recurring winter deep convection, whose extent, strength, and magnitude has been associated with variations in the NAO (e.g., Pickart et al., 2003). The surface sDIC data between January and March in the Irminger Sea as shown in Figure 4a reveal a significant correlation at the 95% level ( $p$  value < 0.05) with the December to March (DJFM)-NAO index (correlation coefficient of 0.61; Hurrell & National Center for Atmospheric Research Staff (Eds), 2017) and with the winter mixed layer depth (MLD, correlation coefficient of 0.84), which was calculated following Pickart et al. (2002). January to March  $f\text{CO}_2$  data show slightly weaker correlations to NAO and MLD, mainly because  $f\text{CO}_2$  is additionally affected by warming, cooling and alkalinity changes. The correlations between sDIC and  $f\text{CO}_2$  with MLD and NAO are most evident in the Irminger Sea and become less significant over the RR and basically nonexistent in the Iceland Basin and further east, where winter mixing is generally shallow and the influence of the state of the NAO on surface ocean biogeochemistry is less pronounced (Figure S9). Note that December data were omitted for these correlation calculations due to the lagged response of the ocean toward atmospheric forcing (e.g., MLDs are deepest by the end of winter).

During a positive phase of the NAO, a substantial sea-air heat loss leads to colder SSTs as well as deeper MLDs (Hurrell & Deser, 2009). During such cold winters, cooling will counteract the  $f\text{CO}_2$  increase driven by sDIC increase. Deep water masses enriched in sDIC and nutrients are brought to the surface, which results in a positive anomaly in sDIC. If the NAO is in a neutral or negative state, winter mixing is generally more shallow and lower sDIC is observed. This negative sDIC anomaly is likely a consequence of marine biological productivity, which reduces the surface ocean in sDIC over summer. During low-phase NAO winters, the pool of sDIC and nutrients in the surface ocean is not fully replenished. A one-dimensional mixing model confirms that the winter sDIC surface concentration can indeed be predicted by integrating the average summer DIC concentration over the winter MLD. The model was initialized each summer using averaged profiles of DIC, temperature, and salinity (i.e., water mass structure) determined from available observations between 2004 and 2017 (García-Ibáñez et al., 2016; Key et al., 2015; Olsen et al., 2016), and run over each winter based on the changes in maximum winter MLD as determined using Argo data (see supporting information for further details). The calculated and measured surface sDIC concentrations reached by the time of the maximum MLD, that is, by the end of winter, agree well (Figure 4b).

## 6. Conclusion

Surface ocean biogeochemistry in the North Atlantic is sensitive to the year-to-year variability in the physical state of the ocean driven by the atmosphere, the large-scale oceanic circulation, and the long-term trends in atmospheric  $\text{CO}_2$ . The strength of the subpolar gyre experiences substantial interannual variability (e.g., Chafik et al., 2016; Häkkinen & Rhines, 2004; Reverdin, 2010; Tesdal et al., 2018), partly in response to the NAO, the leading mode of atmospheric variability over the subpolar North Atlantic (Hurrell & Deser, 2009). In the subpolar North Atlantic a freshening and cooling has occurred after 2005 (Robson et al., 2016; Tesdal et al., 2018), which is suggested to have been induced by negative density anomalies resulting from the post-1995 decadal subpolar gyre warming (Häkkinen & Rhines, 2004; Hátún et al., 2005; Robson et al., 2014). Following the period of warming and increasing salinity in the 1990s, SSTs and SSS started to decline as a result of reduced northward transport of heat and salt due to a reduced strength of the large-scale ocean circulation (Smeed et al., 2018). Measurements on Nuka Arctica confirm a substantial winter cooling from 2004 to 2017 and simultaneously a freshening in the Iceland Basin. Here, the freshwater input is not a locally generated feature, but a signature of decadal overturning circulation variability in the North Atlantic (Smeed et al., 2018; Zhang, 2008; Zhang & Zhang, 2015). The large-scale decadal freshening signal traces the upper ocean North Atlantic Ocean circulation, which is most likely why the pronounced freshening predominantly affects the Iceland Basin.

The ongoing freshening in the subpolar North Atlantic has not yet affected the surface ocean trend in  $f\text{CO}_2$  but could potentially impact water column stratification in a way that likely will reduce vertical fluxes of nutrients and carbon. In the western subpolar North Atlantic, the carbon cycle exhibits large interannual variability with respect to the magnitude of winter mixing. In the western Irminger Sea,  $f\text{CO}_2$  rose at a rate of  $2.8 \mu\text{atm}/\text{year}$  between 1993 and 2003, attributed to a strong surface warming associated with a weaker state of the NAO (Corbière et al., 2007), while between 2001 and 2008, the rate was even higher,  $5.7 \mu\text{atm}/\text{year}$ , mainly driven by changes in the  $\text{CO}_2$  system in seawater and proposed to be the result of changes in vertical mixing processes (Metzl et al., 2010). Compared to both previous studies, the winter surface  $f\text{CO}_2$  trends decelerated between 2004 and 2017, although a remnant of a larger  $f\text{CO}_2$  trend might be visible in the  $f\text{CO}_2$  data collected on Nuka Arctica before 2007. In contrast to the post-1995 warming period, stronger surface cooling in the west than the east after 2004 led to solubility-driven increase of surface ocean DIC concentrations. Additionally, the measurements collected on Nuka Arctica span a period of several consecutive winters in which deep convection took place in the Irminger Sea, that is, winter mixing exceeded 500 m in the winters 2008, 2009, 2012, 2015, and 2016 (de Jong et al., 2012, 2018; Fröb et al., 2016; Piron et al., 2017; Våge et al., 2009) in response to the state of the NAO. During these winters, high-nutrient-high-sDIC waters from below further increase surface  $f\text{CO}_2$ , such that conditions in the surface ocean vary between supersaturation and undersaturation; that is, the subpolar North Atlantic switches between a weak source to a weak sink of atmospheric  $\text{CO}_2$  during winter.

The results of this study highlight the importance and need not only to collect  $f\text{CO}_2$  data on the VOS network but also to implement observation systems that collect more  $\text{CO}_2$  system variables as well as nutrient data. For example, while salinity measurements are useful to approximate alkalinity, they do not allow investigating the impact of calcium carbonate dissolution changes on alkalinity, which introduces uncertainty.



Nutrient data, on the other hand, may help to delineate trends in surface sDIC and  $f\text{CO}_2$  associated with air-sea gas exchange from those driven by vertical mixing and biological processes. In that respect the most recent extension of the Argo program to include pH, oxygen, and nitrate sensors holds the potential to provide biogeochemical observations that will enable a better understanding of the mechanisms of the North Atlantic  $\text{CO}_2$  sink variability in relation to large-scale climate.

#### Acknowledgments

The authors would like to thank Royal Arctic Lines and the captains and crew of M/V Nuka Arctica for their cooperation and generous help. The authors appreciate support from ICOS-Norway (Norwegian Research Council, 245927). This work was funded by the SNACS project (229752), which is part of the KLIMAFORSK program of the Norwegian Research Council. SSS data derived from the thermosalinograph instrument installed on M/V Nuka Arctica were collected, validated, archived, and made freely available by the French Sea Surface Salinity Observation Service (<http://www.legos.obs-mip.fr/observations/sss/>). The  $f\text{CO}_2$  data are available through the SOCAT database (Bakker et al., 2016) and the ICOS-Norway website (<https://no.icos-cp.eu>). The 58GS20150410 data are available at <https://cchdo.ucsd.edu/cruise/58GS20150410>.

#### References

- Alory, G., Delcroix, T., Téchiné, P., Diverrès, D., Varillon, D., Cravatte, S., & Roubaud, F. (2015). The French contribution to the voluntary observing ships network of sea surface salinity. *Deep Sea Research Part I: Oceanographic Research Papers*, *105*, 1–18. <https://doi.org/10.1016/j.dsr.2015.08.005>
- Bakker, D. C. E., Pfeil, B., O'Brien, K. M., Currie, K. I., Jones, S. D., Landa, C. S., & Woosley, R. (2016). Surface Ocean  $\text{CO}_2$  Atlas (SOCAT) V4. <https://doi.org/10.1594/PANGAEA.866856>
- Chafik, L., Häkkinen, S., England, M. H., Carton, J. A., Nigam, S., Ruiz-Barradas, A., & Miller, L. (2016). Global linkages originating from decadal oceanic variability in the subpolar North Atlantic. *Geophysical Research Letters*, *43*, 10,909–10,919. <https://doi.org/10.1002/2016GL071134>
- Chafik, L., Rossby, T., & Schrum, C. (2014). On the spatial structure and temporal variability of poleward transport between Scotland and Greenland. *Journal of Geophysical Research: Oceans*, *119*, 824–841. <https://doi.org/10.1002/2013JC009287>
- Cooperative Global Atmospheric Data Integration Project (2016). Multi-laboratory compilation of atmospheric carbon dioxide data for the period 1957–2015; obspack\_co2\_1\_GLOBALVIEWplus\_v2.1\_2016\_09\_02. NOAA Earth System Research Laboratory, Global Monitoring Division.
- Corbière, A., Metzl, N., Reverdin, G., Brunet, C., & Takahashi, T. (2007). Interannual and decadal variability of the oceanic carbon sink in the North Atlantic subpolar gyre. *Tellus B*, *59*(2), 168–178. <https://doi.org/10.1111/j.1600-0889.2006.00232.x>
- de Jong, M. F., & de Steur, L. (2016). Strong winter cooling over the Irminger Sea in winter 2014–2015, exceptional deep convection, and the emergence of anomalously low SST. *Geophysical Research Letters*, *43*, 7106–7113. <https://doi.org/10.1002/2016GL069596>
- de Jong, M. F., Oltmanns, M., Karstensen, J., & de Steur, L. (2018). Deep convection in the Irminger Sea observed with a dense mooring array. *Oceanography*, *31*(1), 50–59. <https://doi.org/10.5670/oceanog.2018.109>
- de Jong, M. F., van Aken, H. M., Våge, K., & Pickart, R. S. (2012). Convective mixing in the central Irminger Sea: 2002–2010. *Deep-Sea Research Part I-Oceanographic Research Papers*, *63*, 36–51. <https://doi.org/10.1016/j.dsr.2012.01.003>
- Fay, A. R., & McKinley, G. A. (2013). Global trends in surface ocean  $p\text{CO}_2$  from in situ data. *Global Biogeochemical Cycles*, *27*, 541–557. <https://doi.org/10.1002/gbc.20051>
- Feely, R., Takahashi, T., Wanninkhof, R., McPhaden, M., Cosca, C., Sutherland, S., & Carr, M. E. (2006). Decadal variability of the air-sea  $\text{CO}_2$  fluxes in the equatorial Pacific Ocean. *Journal of Geophysical Research*, *111*, C08S90. <https://doi.org/10.1029/2005JC003129>
- Friis, K., Körtzinger, A., & Wallace, D. W. R. (2003). The salinity normalization of marine inorganic carbon chemistry data. *Geophysical Research Letters*, *30*(2), 1085. <https://doi.org/10.1029/2002GL015898>
- Fröb, F., Olsen, A., Våge, K., Moore, K., Yashayaev, I., Jeansson, E., & Rajasakaren, B. (2016). Irminger Sea deep convection injects oxygen and anthropogenic carbon to the ocean interior. *Nature Communications*, *7*, 13244. <https://doi.org/10.1038/ncomms13244>
- García-Ibáñez, M. I., Zunino, P., Fröb, F., Carracedo, L. I., Ríos, A., Mercier, H., & Pérez, F. F. (2016). Ocean acidification in the subpolar North Atlantic: Mechanisms controlling pH changes. *Biogeosciences*, *13*, 3701–3715. <https://doi.org/10.5194/bg-13-3701-2016>
- Gruber, N. (2009). Carbon cycle: Fickle trends in the ocean. *Nature*, *458*, 155–156.
- Gruber, N., Keeling, C., & Bates, N. (2002). Interannual variability in the North Atlantic Ocean carbon sink. *Science*, *298*(5602), 2374–2378. <https://doi.org/10.1126/science.1077077>
- Häkkinen, S., & Rhines, P. (2004). Decline of subpolar North Atlantic circulation during the 1990s. *Science*, *304*(5670), 555–559. <https://doi.org/10.1126/science.1094917>
- Hátún, H., Sando, A., Drange, H., Hansen, B., & Valdimarsson, H. (2005). Influence of the Atlantic subpolar gyre on the thermohaline circulation. *Science*, *309*(5742), 1841–1844. <https://doi.org/10.1126/science.1114777>
- Heinze, C., Meyer, S., Goris, N., Anderson, L., Steinfeldt, R., Chang, N., & Bakker, D. C. E. (2015). The ocean carbon sink—Impacts, vulnerabilities and challenges. *Earth System Dynamics*, *6*(1), 327–358. <https://doi.org/10.5194/esd-6-327-2015>
- Henson, S. A., Painter, S. C., Penny Holliday, N., Stinchcombe, M. C., & Giering, S. L. C. (2013). Unusual subpolar North Atlantic phytoplankton bloom in 2010: Volcanic fertilization or North Atlantic Oscillation? *Journal of Geophysical Research: Oceans*, *118*, 4771–4780. <https://doi.org/10.1002/jgrc.20363>
- Henson, S. A., Robinson, I., Allen, J. T., & Waniek, J. J. (2006). Effect of meteorological conditions on interannual variability in timing and magnitude of the spring bloom in the Irminger Basin, North Atlantic. *Deep Sea Research Part I: Oceanographic Research Papers*, *53*(10), 1601–1615. <https://doi.org/10.1016/j.dsr.2006.07.009>
- Hurrell, J., & Deser, C. (2009). North Atlantic climate variability: The role of the North Atlantic Oscillation. *Journal of Marine Systems*, *78*, 28–41. <https://doi.org/10.1016/j.jmarsys.2008.11.026>
- Hurrell, J., & National Center for Atmospheric Research Staff (Eds.) (2017). The climate data guide: Hurrell North Atlantic Oscillation (NAO) index (station-based). Last modified 07 Nov 2017.
- Keeling, C. D., Brix, H., & Gruber, N. (2004). Seasonal and long-term dynamics of the upper ocean carbon cycle at Station ALOHA near Hawaii. *Global Biogeochemical Cycles*, *18*, GB4006. <https://doi.org/10.1029/2004GB002227>
- Key, R. M., Olsen, A., van Heuven, S., Lauvset, S. K., Velo, A., Lin, X., & Suzuki, T. (2015). *Global ocean data analysis project, version 2 (GLODAPv2)*, ORNL/CDIAC-162, NDP-093. Oak Ridge, TN: Carbon Dioxide Information Analysis Center, Oak Ridge National Laboratory.
- Knutsen, Ø., Svendsen, H., Østerhus, S., Rossby, T., & Hansen, B. (2005). Direct measurements of the mean flow and eddy kinetic energy structure of the upper ocean circulation in the NE Atlantic. *Geophysical Research Letters*, *32*, L14604. <https://doi.org/10.1029/2005GL023615>
- Landschützer, P., Gruber, N., & Bakker, D. C. E. (2016). Decadal variations and trends of the global ocean carbon sink. *Global Biogeochemical Cycles*, *30*, 1396–1417. <https://doi.org/10.1002/2015GB005359>

- Landschützer, P., Gruber, N., Bakker, D. C. E., Schuster, U., Nakaoka, S., Payne, M. R., & Zeng, J. (2013). A neural network-based estimate of the seasonal to inter-annual variability of the Atlantic Ocean carbon sink. *Biogeosciences*, *10*(11), 7793–7815. <https://doi.org/10.5194/bg-10-7793-2013>
- Landschützer, P., Gruber, N., Haumann, F. A., Rödenbeck, C., Bakker, D. C. E., van Heuven, S., & Wanninkhof, R. (2015). The reinvigoration of the Southern Ocean carbon sink. *Science*, *349*(6253), 1221–1224. <https://doi.org/10.1126/science.aab2620>
- Le Quéré, C., Andrew, R. M., Friedlingstein, P., Sitch, S., Hauck, J., Pongratz, J., & Zheng, B. (2018). Global carbon budget 2018. *Earth System Science Data*, *10*(4), 2141–2194. <https://doi.org/10.5194/essd-10-2141-2018>
- Le Quéré, C., Rödenbeck, C., Buitenhuis, E. T., Conway, T. J., Langenfelds, R., Gomez, A., & Heimann, M. (2007). Saturation of the Southern Ocean CO<sub>2</sub> sink due to recent climate change. *Science*, *316*(5832), 1735–1738. <https://doi.org/10.1126/science.1136188>
- Lewis, E., & Wallace, D. W. R. (1998). *Program developed for CO<sub>2</sub> system calculations*. Oak Ridge, TN: ORNL/CDIAC-105. Carbon Dioxide Information Analysis Center, Oak Ridge National Laboratory, US Department of Energy.
- Lovenduski, N. S., Gruber, N., Doney, S. C., & Lima, I. D. (2007). Enhanced CO<sub>2</sub> outgassing in the Southern Ocean from a positive phase of the Southern Annular Mode. *Global Biogeochemical Cycles*, *21*, GB2026. <https://doi.org/10.1029/2006GB002900>
- Lueker, T. J., Dickson, A. G., & Keeling, C. D. (2000). Ocean pCO<sub>2</sub> calculated from dissolved inorganic carbon, alkalinity, and equations for K<sub>1</sub> and K<sub>2</sub>: Validation based on laboratory measurements of CO<sub>2</sub> in gas and seawater at equilibrium. *Marine Chemistry*, *70*, 105–119. [https://doi.org/10.1016/S0304-4203\(00\)00022-0](https://doi.org/10.1016/S0304-4203(00)00022-0)
- Marotzke, J., Christian Jakob, S. B., Dirmeyer, P. A., O’Gorman, P. A., Hawkins, E., Perkins-Kirkpatrick, S., & Tuma, M. (2017). Climate research must sharpen its view. *Nature Climate Change*, *7*, 89–91. <https://doi.org/10.1038/nclimate3206>
- McKinley, G. A., Fay, A. R., Takahashi, T., & Metzl, N. (2011). Convergence of atmospheric and North Atlantic carbon dioxide trends on multidecadal timescales. *Nature Geoscience*, *4*(9), 606–610. <https://doi.org/10.1038/ngeo1193>
- Metzl, N., Corbiere, A., Reverdin, G., Lenton, A., Takahashi, T., Olsen, A., & Ramonet, M. (2010). Recent acceleration of the sea surface fCO<sub>2</sub> growth rate in the North Atlantic subpolar gyre (1993–2008) revealed by winter observations. *Global Biogeochemical Cycles*, *24*, GB4004. <https://doi.org/10.1029/2009GB003658>
- Millero, F. J., Feistel, R., Wright, D. G., & McDougall, T. J. (2008). The composition of standard seawater and the definition of the reference-composition salinity scale. *Deep Sea Research Part I: Oceanographic Research Papers*, *55*(1), 50–72. <https://doi.org/10.1016/j.dsr.2007.10.001>
- Millero, F. J., Lee, K., & Roche, M. (1998). Distribution of alkalinity in the surface waters of the major oceans. *Marine Chemistry*, *60*(1–2), 111–130. [https://doi.org/10.1016/S0304-4203\(97\)00084-4](https://doi.org/10.1016/S0304-4203(97)00084-4)
- Nondal, G., Bellerby, R. G. J., Olsen, A., Johannessen, T., & Olafsson, J. (2009). Optimal evaluation of the surface ocean CO<sub>2</sub> system in the northern North Atlantic using data from voluntary observing ships. *Limnology and Oceanography: Methods*, *7*(1), 109–118. <https://doi.org/10.4319/lom.2009.7.109>
- Olsen, A., Brown, K. R., Chierici, M., Johannessen, T., & Neill, C. (2008). Sea-surface CO<sub>2</sub> fugacity in the subpolar North Atlantic. *Biogeosciences*, *5*(2), 535–547. <https://doi.org/10.5194/bg-5-535-2008>
- Olsen, A., Key, R. M., van Heuven, S., Lauvset, S. K., Velo, A., Lin, X., & Suzuki, T. (2016). The global ocean data analysis project version 2 (GLODAPv2)—An internally consistent data product for the world ocean. *Earth System Science Data*, *8*(2), 297–323. <https://doi.org/10.5194/essd-8-297-2016>
- Pickart, R., Straneo, F., & Moore, G. (2003). Is Labrador Sea water formed in the Irminger basin? *Deep-Sea Research Part I-Oceanographic Research Papers*, *50*(1), 23–52. [https://doi.org/10.1016/S0967-0637\(02\)00134-6](https://doi.org/10.1016/S0967-0637(02)00134-6)
- Pickart, R., Torres, D., & Clarke, R. (2002). Hydrography of the Labrador Sea during active convection. *Journal of Physical Oceanography*, *32*(2), 428–457. <https://doi.org/10.21236/ada609735>
- Pierrot, D., Neill, C., Sullivan, K., Castle, R., Wanninkhof, R., Lüger, H., & Cosca, C. E. (2009). Recommendations for autonomous underway pCO<sub>2</sub> measuring systems and data-reduction routines. *Deep Sea Research Part II: Topical Studies in Oceanography*, *56*(8), 512–522. <https://doi.org/10.1016/j.dsr2.2008.12.005>
- Piron, A., Thierry, V., Mercier, H., & Caniaux, G. (2017). Gyre-scale deep convection in the subpolar North Atlantic Ocean during winter 2014–2015. *Geophysical Research Letters*, *44*, 1439–1447. <https://doi.org/10.1002/2016GL071895>
- Reverdin, G. (2010). North Atlantic subpolar gyre surface variability (1895–2009). *Journal of Climate*, *23*(17), 4571–4584. <https://doi.org/10.1175/2010JCLI3493.1>
- Reverdin, G., Valdimarsson, H., Alory, G., Diverres, D., Bringas, F., Goni, G., & Friedman, A. R. (2018). North Atlantic subpolar gyre along predetermined ship tracks since 1993: A monthly data set of surface temperature, salinity, and density. *Earth System Science Data*, *10*(3), 1403–1415. <https://doi.org/10.5194/essd-10-1403-2018>
- Robson, J., Hodson, D., Hawkins, E., & Sutton, R. (2014). Atlantic overturning in decline? *Nature Geoscience*, *7*, 2–3. <https://doi.org/10.1038/ngeo2050>
- Robson, J., Ortega, P., & Sutton, R. (2016). A reversal of climatic trends in the North Atlantic since 2005. *Nature Geoscience*, *9*, 513–517. <https://doi.org/10.1038/ngeo2727>
- Rödenbeck, C., Bakker, D. C. E., Gruber, N., Iida, Y., Jacobson, A. R., Jones, S., & Zeng, J. (2015). Data-based estimates of the ocean carbon sink variability—First results of the surface ocean pCO<sub>2</sub> mapping intercomparison (SOCOM). *Biogeosciences*, *12*(23), 7251–7278. <https://doi.org/10.5194/bg-12-7251-2015>
- Rödenbeck, C., Bakker, D. C. E., Metzl, N., Olsen, A., Sabine, C., Cassar, N., & Heimann, M. (2014). Interannual sea-air CO<sub>2</sub> flux variability from an observation-driven ocean mixed-layer scheme. *Biogeosciences*, *11*(17), 4599–4613. <https://doi.org/10.5194/bg-11-4599-2014>
- Schuster, U., & Watson, A. J. (2007). A variable and decreasing sink for atmospheric CO<sub>2</sub> in the North Atlantic. *Journal of Geophysical Research*, *112*, C11006. <https://doi.org/10.1029/2006JC003941>
- Smeed, D. A., Josey, S. A., Beaulieu, C., Johns, W. E., Moat, B. I., Frajka-Williams, E., & McCarthy, G. D. (2018). The North Atlantic Ocean is in a state of reduced overturning. *Geophysical Research Letters*, *45*, 1527–1533. <https://doi.org/10.1002/2017GL076350>
- Takahashi, T., Olfsson, J., Goddard, J. G., Chipman, D. W., & Sutherland, S. C. (1993). Seasonal variation of CO<sub>2</sub> and nutrients in the high-latitude surface oceans: A comparative study. *Global Biogeochemical Cycles*, *7*(4), 843–878. <https://doi.org/10.1029/93GB02263>
- Takahashi, T., Sutherland, S. C., Wanninkhof, R., Sweeney, C., Feely, R. A., Chipman, D. W., & de Baar, H. J. (2009). Climatological mean and decadal change in surface ocean pCO<sub>2</sub>, and net sea-air CO<sub>2</sub> flux over the global oceans. *Deep Sea Research Part II: Topical Studies in Oceanography*, *56*(8–10), 554–577. <https://doi.org/10.1016/j.dsr2.2008.12.009>
- Tesdal, J. E., Abernathy, R. P., Goes, J. I., Gordon, A. L., & Haine, T. W. N. (2018). Salinity trends within the upper layers of the subpolar North Atlantic. *Journal of Climate*, *31*(7), 2675–2698. <https://doi.org/10.1175/JCLI-D-17-0532.1>
- Thomas, H., Prowe, A. E. F., Lima, I. D., Doney, S. C., Wanninkhof, R., Greatbatch, R. J., & Corbiere, A. (2008). Changes in the North Atlantic Oscillation influence CO<sub>2</sub> uptake in the North Atlantic over the past 2 decades. *Global Biogeochemical Cycles*, *22*, GB4027. <https://doi.org/10.1029/2007GB003167>

- Tjiputra, J., Olsen, A., Bopp, L., Lenton, A., Pfeil, B., Roy, T., & Heinze, C. (2014). Long-term surface  $p\text{CO}_2$  trends from observations and models. *Tellus B*, *66*, 23083. <https://doi.org/10.3402/tellusb.v66.23083>
- United Nations Framework Convention on Climate Change (2015). Adoption of the Paris agreement. In *21st Conference of the Parties* (2 p.). Paris: United Nations.
- Våge, K., Pickart, R. S., Thierry, V., Reverdin, G., Lee, C. M., Petrie, B., & Ribergaard, M. H. (2009). Surprising return of deep convection to the subpolar North Atlantic Ocean in winter 2007–2008. *Nature Geoscience*, *2*(1), 67–72. <https://doi.org/10.1038/NGEO382>
- van Heuven, S., Pierrot, D., Rae, J., Lewis, E., & Wallace, D. (2011). MATLAB program developed for  $\text{CO}_2$  system calculations, ORNL/CDIAC-105b. Carbon Dioxide Information Analysis Center, Oak Ridge National Laboratory, US Department of Energy, Oak Ridge, TN.
- Wanninkhof, R., Park, G. H., Takahashi, T., Sweeney, C., Feely, R., Nojiri, Y., & Khatiwala, S. (2013). Global ocean carbon uptake: Magnitude, variability and trends. *Biogeosciences*, *10*(3), 1983–2000. <https://doi.org/10.5194/bg-10-1983-2013>
- Weiss, R., & Price, B. (1980). Nitrous oxide solubility in water and seawater. *Marine Chemistry*, *8*, 347–359. [https://doi.org/10.1016/0304-4203\(80\)90024-9](https://doi.org/10.1016/0304-4203(80)90024-9)
- Zhang, R. (2008). Coherent surface-subsurface fingerprint of the Atlantic meridional overturning circulation. *Geophysical Research Letters*, *35*, L20705. <https://doi.org/10.1029/2008GL035463>
- Zhang, J., & Zhang, R. (2015). On the evolution of Atlantic Meridional Overturning Circulation fingerprint and implications for decadal predictability in the North Atlantic. *Geophysical Research Letters*, *42*, 5419–5426. <https://doi.org/10.1002/2015GL064596>